AIAA JOURNAL
Vol. 32, No. 5, May 1994

Structure of Local Pressure-Driven Three-Dimensional Transient Boundary-Layer Separation

Laura L. Pauley*
Pennsylvania State University, University Park, Pennsylvania 16802

The separation of a flat-plate, laminar boundary layer under the influence of a suddenly imposed three-dimensional external adverse pressure gradient was studied computationally by time-accurate numerical solution of the incompressible Navier-Stokes equations. The separation decay was then investigated by impulsively removing the pressure gradient. The development and decay of the separation structure were compared with experimental results reported by other investigators for the same geometry. The periodic vortex shedding of the three-dimensional separation was described in terms of a Strouhal number based on the freestream velocity and Blasius boundary-layer momentum thickness at the location where separation occurs. The characteristic Strouhal number of 0.0136 during the separation development from the computation compared favorably with 0.0134 from the experiment. When the adverse pressure gradient was impulsively removed, the boundary layer returned to an attached boundary layer much faster than the time required for the separation development.

I. Introduction

THE behavior of a boundary layer growing along the surface of a body in a viscous flow is greatly influenced by the imposed pressure distribution. If the pressure rises in the flow direction (an adverse pressure gradient), then, as first noted by Prandtl,[1] the fluid near the wall will be retarded more than the freestream fluid and may undergo boundary-layer separation. In all practical situations the flow is three dimensional, and its structure in the separation zone is topologically complex and often unsteady. Three-dimensional and unsteady flows have not been accurately described by models for stationary, two-dimensional separation. It is important to know when separation will occur, to understand the structure of separated flows, and to predict the time required for development or decay of the separation.

The objective of the present study is to establish the structure and time scales present in the development and decay of a three-dimensional separation produced by a localized adverse pressure gradient. The current investigation is the numerical portion of a combined experimental and computational study of unsteady three-dimensional separation in a very simple and well-controlled geometry. The adverse pressure gradient was impulsively applied and removed so that the inherent time scales for growth and decay could be studied. During the development and decay, the changing topological structure of the separation was studied. In separate cases, the adverse pressure gradient was removed at three different times during the separation development. This established the conditions when the separation was recoverable and when it was catastrophic. Although the geometry was very simple, the results provide general insight into the structure and scaling of three-dimensional boundary-layer separation, which can be applied to applications such as three-dimensional bodies in an unsteady flow and pitching three-dimensional bodies.

The computation provided detailed information but was only conducted at one set of flow conditions because the unsteady, three-dimensional study was computationally intensive. In the companion experiment, selected velocity measurements were made to describe the development of the separation for several flow velocities and pressure gradient strengths. Flow visualization was also used to supply a qualitative description of the separation structure. The experimental results are reported in Henk et al.,[2] herein referred to as HRR.

Several different techniques were used to investigate the separation structure in detail. Unsteady velocity profiles across the boundary layer and velocity histories along the centerline of the channel at select streamwise locations were considered. The computational results were also studied using streamlines in the flow, limiting streamlines, streamlines of projected velocity vectors onto a cross plane, and vorticity lines. Comparison was made to the experimental results described in HRR.

II. Background

The topology of limiting streamlines at the surface of a body is useful for conceptual study of three-dimensional separation (Maskell[3] and Oswatitsch[4]). For steady flows, these lines can be visualized experimentally using a surface oil film technique. Although these surface lines give important information about the separation region, they sometimes fail to detect important features of the flow away from the wall and therefore they should be examined only as a first step in the study of a three-dimensional separation.

Singular points in the limiting streamline topology occur where more than one streamline passes through the point. Two streamlines pass through a saddle point, whereas an infinite number of streamlines pass through a node or focus. Legendre,[5] Davey,[6] and Lighthill[7] discussed the combinations of these singularities that can occur on a surface. For any simply connected three-dimensional surface there must be two more nodes (and foci) than saddle points when global separation occurs. Wang[8] uses the term "closed separation" to refer to the structure termed "global separation" by Tobak and Peake.[9] In three dimensions, the line of separation is defined as the line upon which limiting streamlines converge. At this line, the fluid that has traveled nearly parallel to the surface is forced to suddenly lift away due to the convergence of streamlines. The flow direction before separation gives the direction of flow along the separation line. When global separation occurs, the separation line originates at a saddle point of separation. Tobak and Peake[9] refer to extensions of the separation line into the entire flowfield as "dividing surfaces." It is instructive to consider the lines of separation and then to investigate the dividing surfaces, which help to identify where fluid is entrained and expelled.

Topological techniques have also been applied in planes passing through the flow. For example, Perry and Fairlie[10] and Hunt et al.[11] considered planes that cut the flow and drew

Received July 26, 1993; revision received Nov. 2, 1993; accepted for publication Nov. 8, 1993.

*Assistant Professor, Department of Mechanical Engineering. Member AIAA.

the streamlines produced by the in-plane velocity components. These results must be interpreted carefully because only in the case of a plane of symmetry with no normal velocity component will these velocity lines correspond to the actual streamlines. Although the lines are not usually streamlines, they can indicate the flow structure found in that plane, and we will find this useful in examining the present simulation. For details of the topological analysis of three-dimensional separation, see Tobak and Peake[9] and Perry and Chong.[12]

Many studies of three-dimensional separation can be found, although most have investigated steady separation structures. The diversity of streamline patterns can be seen in reviews by Peake and Tobak,[13] Bippes,[14] and Werlé.[15] For bodies of revolution, different topologies have been observed depending on the geometry of the body and the angle of attack. Peake and Tobak[16] studied the topological structures formed about a cylinder with a spherical head at various angles of attack up to 32.5 deg. Using oil flow and a crossflow laser sheet for flow visualization, they observed a structure described as an "owl-face of the first kind" by Perry and Chong.[17] Studies at subsonic and supersonic freestream velocities resulted in the same topological structure.

Numerical studies of three-dimensional separation require large computational capability and have not been possible until recently. Current computational facilities allow calculations of the full flowfield about a body using the Navier-Stokes equations. For example, Ying et al.[18] studied the steady, supersonic, laminar flow about a hemisphere-cylinder at the conditions studied by Peake and Tobak.[16] When the experimental visualization techniques were duplicated computationally, many of the same topological structures were found. More recently, Wang and Hsieh[19] also computationally studied the flow structure about a hemisphere-cylinder at high angles of incidence.

Unsteady separation has been studied both experimentally and numerically. Most research to date has focused on two-dimensional separation and considered an oscillating freestream or body. Reviews of unsteady separation research include McCroskey,[20] Telionis,[21] and Reynolds and Carr.[22] Recent unsteady three-dimensional separation studies are described in Moffatt and Tsinober[23] and Dallmann.[24,25]

III. Problem Definition

A. Geometry

The geometry of the present computational study and dimensions of the facility used in the companion experimental study are shown in Fig. 1. The geometry was designed to produce a localized separation with well-described boundary conditions. This allowed the conditions from the companion experiment to be easily quantified and then matched in the computations. Throughout the entire development and decay of the separation, the freestream velocity upstream remained uniform and steady. The laminar boundary layer on one wall (the "test wall"), which developed under zero pressure gradient, was exposed to a sudden local adverse pressure gradient by suction through a square port on the opposite wall (the "control wall"). The same geometry and flow conditions were used in the computation. The test section was 0.129 m high and 0.356 m wide. The upstream edge of the suction port was located 0.613 m downstream of the test plate leading edge and was 3.8 cm square. Further details of the experimental facility can be found in HRR.

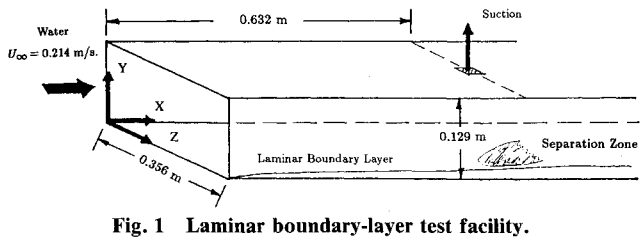

Fig. 1 Laminar boundary-layer test facility.

The strength of the pressure gradient was set such that the boundary layer of the test wall would separate. The separated boundary layer never exceeded 20% of the channel height, thus effectively producing an external boundary-layer flow with an imposed pressure gradient. Therefore, the response of the boundary layer was rather insensitive to the manner with which the adverse pressure gradient was imposed. The pressure gradient was impulsively applied and removed to distinguish between the fast and slow responses. In the two-dimensional separation studies of Pauley et al.,[26] herein denoted as PMR, it was found that a slow exponentially applied adverse pressure gradient increased the development time of the separation but did not change the ultimate structure. The experimental investigation of HRR found that a slowly applied three-dimensional pressure gradient would produce a separation growth similar in structure to that observed in the present study.

B. Numerical Computation

The fractional time step method developed by Kim and Moin[27] was used to solve the unsteady incompressible Navier-Stokes equations with constant viscosity. The method is second-order accurate in space and time. The present computational study is a direct numerical simulation of all resolvable structures. No turbulence modeling was applied. The computation contained 256 points in the streamwise direction, 128 points in the normal direction, and 64 points in the spanwise direction. The flow variables are nondimensionalized using the channel height h and upstream approach velocity u_0. Lower-case symbols are dimensional quantities and capital letters denote nondimensional variables. For example, $X = x/h$, $Y = y/h$, $U = u/u_0$, and $T = tu_0/h$. The upstream edge of the suction port is at $X = 4.75$, and the port extends to $X = 5.05$. The channel centerline is at $Z = 1.38$.

Half of the grid points were clustered in the 20% of the domain near the test wall using a hyperbolic tangent distribution. Throughout the computation, the entire separation structure remained within the region of well-refined grid resolution. Uniform grid spacing was applied in the streamwise and spanwise directions. The grid independence of the solution was tested for a two-dimensional separation by doubling the number of grid points in the streamwise and normal directions independently; for both cases the changes in the flow velocity and shedding frequency were less than 0.5% (see PMR). Since the three-dimensional separation was similar in height and length, it was therefore expected that the same computational grid will produce a grid-independent result.

Computations with a refined three-dimensional grid were not possible due to the computational intensity of three-dimensional computations. The spanwise grid resolution, however, was tested by halving the number of spanwise grid points. For $T < 5.0$, the velocity fields produced by the two grids differed by less than 5%. At later times in the computation, the three-dimensionality of the flowfield increased, and the reduced grid resolution domain produced higher relative errors in velocity near singular points in the flow topology, where low velocities exist. However, throughout the entire development of the separation structure, the reduced grid containing 32 points in the spanwise direction accurately predicted the separation topology and the location of singular points. Therefore, the computation that used 64 points in the spanwise direction is considered to adequately resolve the spanwise gradients.

A no-slip boundary condition was applied on the test wall, whereas a no-stress boundary condition was used along the control wall to reduce the required resolution in this region. Because the no-stress boundary condition prescribes a zero vorticity boundary, a boundary layer does not develop along the control wall. A parabolic variation of the suction velocity was assumed in both directions to make the wall-normal velocity continuous along the control wall so as to avoid strong local gradients. Periodic boundary conditions were used in the spanwise direction. Although this boundary condition does

not impose solid side walls, the solution was symmetric, and the spanwise velocity was zero at the spanwise boundaries. The side boundaries therefore acted as no-stress solid walls.

The velocity profile at the inlet to the domain was prescribed as a Blasius boundary layer of the proper thickness under a steady uniform external flow. The inlet boundary of the domain was set at a location where the inviscid flowfield varied by less than 2% from wall to wall across the channel. Various exit boundary conditions were tested, and it was found that the convective exit boundary conditions

$$\frac{\partial u}{\partial t} + c\frac{\partial u}{\partial x} = 0 \tag{1a}$$

$$\frac{\partial v}{\partial t} + c\frac{\partial v}{\partial x} = 0 \tag{1b}$$

$$\frac{\partial w}{\partial t} + c\frac{\partial w}{\partial x} = 0 \tag{1c}$$

allowed the propagating vortex to exit the domain with little distortion. The propagation speed of the vortices within the computational domain gave the value for c. To within 0.2%, the same computational results were obtained when the average exit velocity was used for c, and hence the value of c was not critical to the numerical solution. To test the influence of the exit boundary location on the computational results, the length of the domain was extended in a two-dimensional separation study (see PMR). The computational domain was 50% larger and contained 50% more grid points in the streamwise direction, retaining the same grid spacing. Near the exit of the short domain, the results of the two computations differed by up to 3%. However, the results at locations more than one channel height upstream of the exit plane differed by less than 0.2%. Thus, the results of interest were essentially independent of the domain truncation.

The initial field was prescribed as the steady-state solution in the channel with no suction applied. Suction was impulsively applied at $T = 0$. The time step for the computation was $\Delta T = 4.0 \times 10^{-4}$. To check the time step independence of the solution, two shedding cycles in the three-dimensional geometry were computed using $\Delta T = 2.0 \times 10^{-4}$. The flow velocities and shedding frequencies for the two step sizes differed by at most 0.5%. Each time step of the computation required 52 s on a CRAY2 computer.

Because three-dimensional, unsteady numerical studies are computationally intensive, only one case was investigated. Flow visualization in the experimental facility was used to determine conditions that yield a three-dimensional separation structure with periodic vortex shedding. The computation was run at $u_0 = 0.214$ m/s, and 16% of the throughflow was removed at the suction port. This resulted in a maximum streamwise pressure gradient of $\partial C_p/\partial x = 2.46$ m^{-1} where $C_p = (P - P_\infty)/\frac{1}{2}\rho U_\infty^2$. The experimental velocity measurements of HRR were made along the centerline of the channel at $u_0 = 0.214$ m/s and 16.4% throughflow removed. The maximum streamwise pressure gradient of the experimental conditions was $\partial C_p/\partial x = 2.52$ m^{-1}. The nominal Reynolds number based on the conditions at the streamwise location where the suction port begins was $Re_x = 1.20544 \times 10^5$. Because the velocity outside the boundary layer varies across the channel, the boundary-layer edge velocity used in the Reynolds number was taken as the slip velocity on the control wall in the absence of suction.

IV. Separation Development

A. Centerline Velocity Profiles and Velocity Histories

After impulsively initiating suction at $T = 0$, a three-dimensional separation began to develop on the test surface. The development of the velocity profile was recorded at several downstream locations in both the computational and experimental studies (HRR). Velocity histories were also recorded at several locations. Two hundred realizations of the velocity profile were ensemble averaged in the experimental studies of HRR.

Figure 2 shows a comparison between the centerline velocity profile development of the computation and experiment at $X = 5.06$. From these results, it can be seen that there is a qualitatively good comparison between the experiment and computation in the time development of the separated velocity profile. Comparisons between computational and experimental velocity profiles at other streamwise locations were similarly favorable. It should be noted that the computation records a single separation event and does not include the ensemble averaging of the unsteady process that is used to obtain the experimental results. The difference between the single event computational results and ensemble-averaged experimental results may be important in the downstream region of the separation and at later times in the separation development ($T < 6.0$) where the unsteadiness is not repeatable over

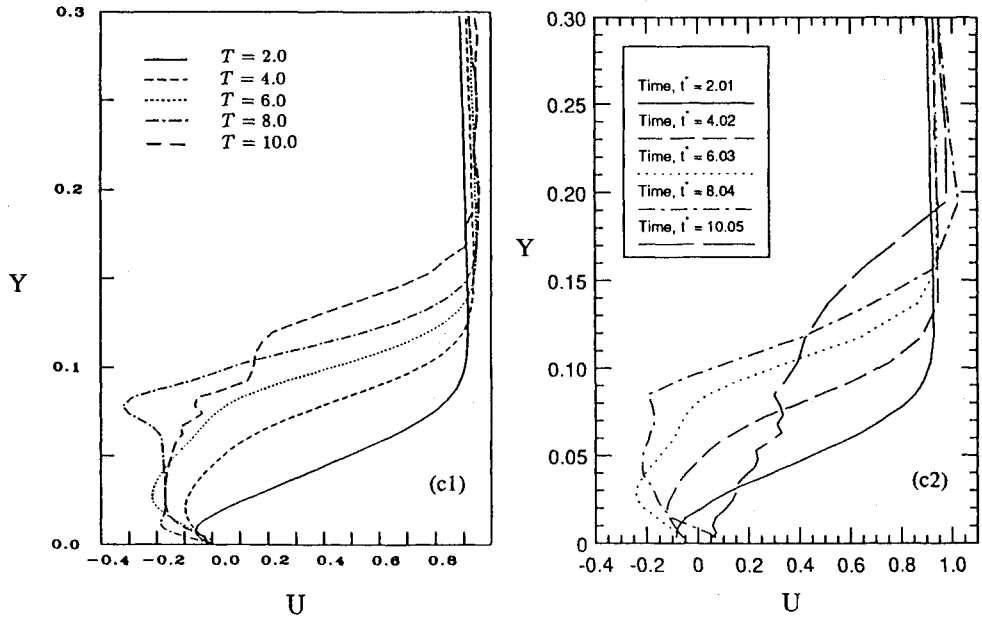

Fig. 2 Streamwise velocity profile at $X = 5.06$ during the separation development. Computational results on the left, ensemble-averaged experimental results of HRR on the right.

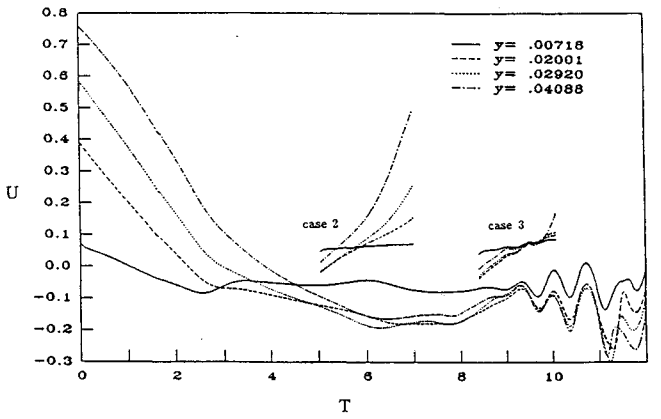

a) $X = 5.06$

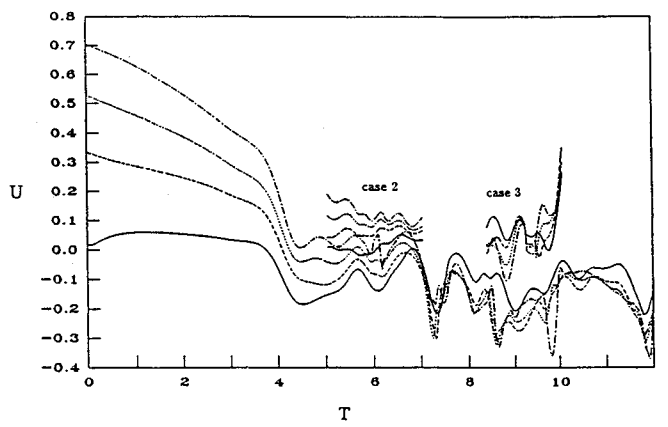

b) $X = 5.65$

Fig. 3 Centerline streamwise velocity histories at four distances from the wall. Included are the velocity histories of the separation growth and the separation decay for cases 2 and 3.

several events. As will be shown later, the separated shear layer becomes unstable in the experimental facility earlier than in the computation. This is probably due to the freestream turbulence and spanwise nonuniformity inherent in the experiment. In the freestream when no adverse pressure gradient is applied, the study of HRR reports that the rms level of streamwise velocity fluctuations was $\sqrt{u'^2}/u_0 \leq 0.6\%$ and the freestream velocity was spanwise uniform to within 2%. The discrepancies between the boundary-layer profiles from the experiment and computation for $T > 6.0$ are most likely due to these phenomena.

The velocity histories along the centerline at $X = 5.06$ and 5.65 are shown in Fig. 3. Also shown are the velocity histories when the adverse pressure gradient was removed. The velocity histories during the separation decay, denoted by "case 2" and "case 3," will be discussed in Sec. V. Oscillations, which first appear in the velocity histories at $X = 5.65$, are due to vortex shedding from the separation during flow development. The oscillations move upstream as the vortex shedding becomes more severe.

As the separation developed, the shear layer lifted away from the wall, the velocity history became oscillatory, and vortex shedding occurred. When taken in a reference frame moving with the shed vortex, instantaneous streamlines move around the shed vortex centerline. Following Yates and Chapman,[28] the vortex centerline was identified as "a streamline within a region of spiralling streamlines that has a minimum curvature." The vortex core refers to the vortex tube surrounding the vortex centerline. The structure of the separated region became more complex and small-scale unsteadiness could be noted by examining the streamlines along the centerline. The size of the smallest scales within the flow decreased as the separation developed. The computation was ended when the smallest structures within the flow could no longer be resolved by the computational grid ($T = 11.5$).

The ensemble-averaged experimental velocity histories at $X = 5.06$ are shown in Fig. 4 for four distances from the test wall where the axes have been rescaled from HRR for comparison with Fig. 3a. Because of the rescaling of the experimental measurements, data from $T = 8.5$–9.2 extend beyond the plot. It can be noted that the separated shear layer becomes unstable in the experimental facility before the computational prediction. This is probably due to the freestream turbulence inherent in the experiment. Transition experiments have shown that freestream turbulence increases the amplitude of the boundary-layer instability and leads to a more rapid development of periodic velocity oscillations within the separated shear layer. The shear layer oscillations may produce transition or may cause the shear layer to roll up and result in vortex shedding. Papers that demonstrate the influence of freestream turbulence on boundary-layer stability include Mack[29] and Narasimha.[30]

The initial vortex shedding frequency can be determined from the computation and experiment by using the first few oscillations of the velocity histories. The initial shedding frequency describes the vortex shedding before small-scale turbulence has developed within the separated region. The vortex shedding frequency of the unsteady separation can be nondimensionalized to form a Strouhal number,

$$St = \frac{f \cdot \theta_0}{u_0} \tag{2}$$

where u_0 and θ_0 are the freestream streamwise velocity and momentum thickness with no applied adverse pressure gradient; u_0 and θ_0 are evaluated at $X = 4.46$, which corresponds to the steady separation point when the adverse pressure gradient is applied. The velocity history for $9.0 < T < 11.5$ from the computation has a characteristic Strouhal number of 0.0136. From the experimental velocity history between $7.0 < T < 13.0$, the Strouhal number was 0.0134. There is good agreement between the Strouhal number from the ensemble-averaged experimental results and the computational results during the separation development.

In the experimental study of HRR, it was found that the initial shedding frequency was only temporary and did not indicate the characteristic frequency after the separation region had reached a maximum size, referred to as quasisteady in HRR. HRR found that the Strouhal number for the quasisteady flow was $St = 0.011 \pm 0.001$ for all Reynolds numbers and pressure gradients tested. The vortex shedding frequency was reduced after the separated shear layer had reached a quasisteady state due to small-scale turbulence within the flow. The quasisteady shedding frequency could not be determined by the present computations since the computational grid could not resolve the small-scale turbulence present in the experimental flow. For this reason, the computation was not continued to a quasisteady condition.

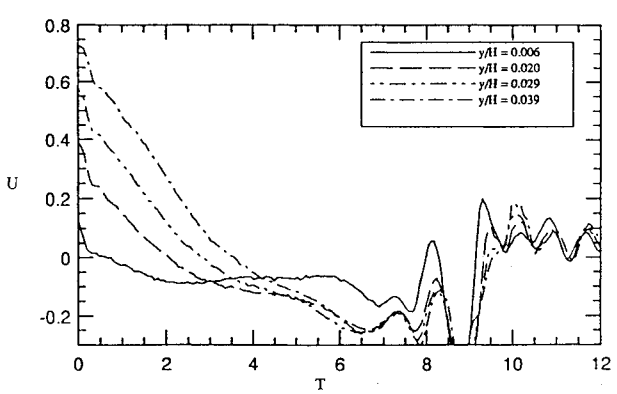

Fig. 4 Centerline experimental ensemble-averaged streamwise velocity histories at four distances from the wall during separation development at $X = 5.06$ (from HRR).

In the two-dimensional numerical study of PMR, which used the centerline geometry of the present investigation, a characteristic shedding frequency of $St = 0.0069$, about half that for the three-dimensional separation, was found for all Reynolds numbers and pressure gradients tested.

B. Topological Development of Limiting Streamlines

The development of the separated region can be studied by considering the limiting streamlines at the wall, which were found using the computational velocity field at the first grid point from the wall, $Y = 0.003$. Figures 5a–5d show the development of the limiting streamlines in time. After impulsively applying the adverse pressure gradient, the attached boundary layer begins to separate. The first topological structure that develops (not shown) contains a node (N) followed by a saddle of reattachment (S) along the centerline. These singularities were found by a search of the velocity field but could not be observed graphically since the singular points were nearly coincident. By $T = 0.05$ the saddle of reattachment has split into a node on the centerline with a saddle on each side. The singular points move apart during the development of the separation as seen in Fig. 5a. The saddles move outward toward the side walls, and the node of separation moves slightly upstream.

The separation topology is consistent with the theorem of Lighthill[7] that states that

$$\sum \text{nodal points} - \sum \text{saddle points} = 2 \qquad (3)$$

Here both nodes and foci are considered nodal points as described by Tobak and Peake.[9] Wang[8] comments that the Lighthill theorem is only to be used for a closed separation, referred to as a global separation by Tobak and Peake. The Lighthill theorem describes the topology on a closed body surrounded by fluid; however, this theorem can be applied to the present geometry by imagining the test plate as a finite body with nodes at the leading and trailing edges and an attached boundary layer under the plate. In addition, the Lighthill theorem was formulated to describe the topology of a steady flowfield. Hui and Tobak[31] have shown that the topology of an unsteady incompressible separation is also described by the Lighthill theorem when viewed from a reference frame fixed to the body surface.

Half-saddles (HS) result when the saddle points reach both side walls at $T = 4.0$ (Fig. 5b). A thin region of flow reversal is now present across the entire channel due to the streamwise adverse pressure gradient extending across the channel. This was also observed in the companion experiment by positioning a laser sheet very close to the test wall. The streamlines in the reversed flow region near the centerline, which converge at the separation node during the early stages of the separation development, become parallel and now diverge. The leading separation node becomes a saddle of separation with one node on either side close to the centerline. These nodes, which will be referred to as the "primary nodes," move away from the centerline. The fixed separation that is described by the saddle point of separation and the primary nodes will be called the "primary separation." The vortex centerline passing through the primary separation is termed the "primary vortex." This new, more complicated structure still satisfies Lighthill's topological theorem.

At later times ($T = 6.0$–8.0) shown in Figs. 5c and 5d, the primary nodes move downstream and toward the centerline. Vortex shedding is identified within the spanwise reversed flow region by the movement of the downstream pair of half-saddle points at the side walls. The term "secondary vortex" will be used to refer to the shed vortex that extends across the span of the channel. The upstream pair of half-saddle points and the primary nodes do not move while shedding of the secondary spanwise vortex occurs. This indicates that the line of separation and the primary spanwise vortex remain stationary. Downstream of the reattachment point the streamlines appear wavy due to the presence of an unstable free shear layer. After $T = 6.0$, the topology of the separation does not change in character but the separation continues to grow in size. The experimental velocity measurements indicate that the

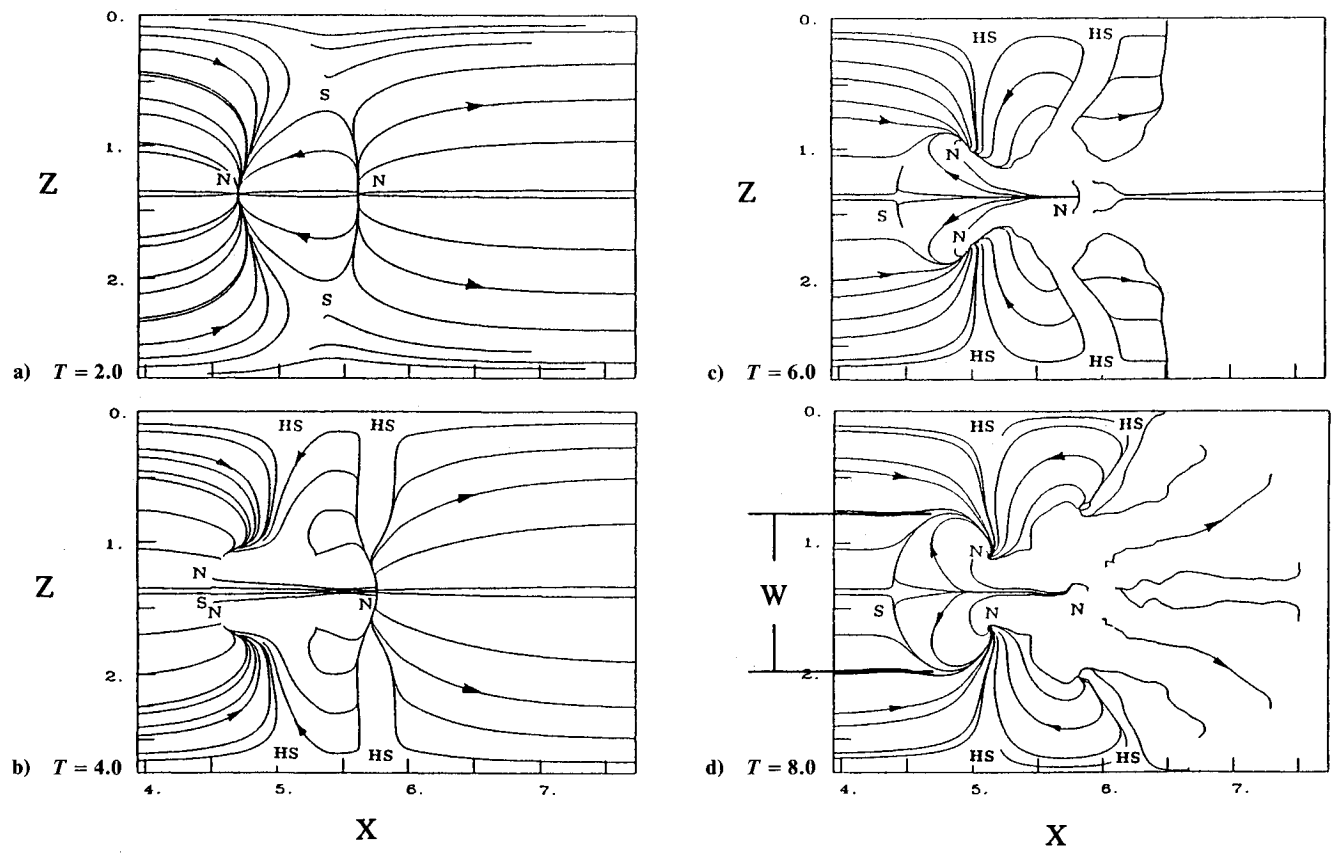

Fig. 5 Limiting streamlines at the test wall.

separation structure reaches a quasisteady state at $T = 14.0$ and ceases to grow further.

The characteristic width of the separation W is a useful parameter in describing the separation growth; W is defined as the maximum distance between the limiting streamlines that originate upstream near the centerline (see Fig. 5d). Since all limiting streamlines originating upstream near the centerline converge as the maximum width is reached, the separation width can be accurately determined. During the early development of the separation, the distance between the foci corresponds to the width of the separation. After $T = 5.0$, the foci move toward the centerline, and the width of the separation continues to increase. The temporal change of the width of the separation and the distance between the nodes is shown in Fig. 6. Included is the distance that the saddle point of separation moves from its initial location at $X = 4.78$. Each measurement is seen to reach an asymptote, indicating that the separation develops to a limiting structure. The size of the limiting structure, however, is probably less than that found for an infinite span channel since the periodic sidewall boundary conditions have likely constrained the growth of the separation.

The development of the topological structure can be described using a convective time for the separation. The convective time T^* is written in terms of the width of the developed separation w_{sep} and the freestream velocity u_0

$$T^* = \frac{tu_0}{w_{sep}} \tag{4}$$

where $w_{sep} = 0.163$ m. Since spatial fluctuations due to the free shear layer are present near the reattachment point, the length of the separation is not well defined, but it is comparable to the width of the separation. Thus $T^* = 1.0$ is the approximate time required for freestream fluid to travel the length of the separation. The development of the separation structure is briefly summarized in Table 1.

The limiting streamline topology of the present study can be compared with results for the separation on a hemisphere-cylinder at angle of attack by Peake and Tobak[16] and Ying et al.[18] The surface topology of Wang and Hsieh[19] for a hemisphere-cylinder at 10-deg angle of attack also agrees with that computed by Ying et al. The steady-flow patterns at different angles of attack up to 10 deg show a progression of topological structures that also appear during the time development of the present computation. The thin spanwise separation observed in the current computation, however, was not present in the hemisphere-cylinder geometry since the spanwise pressure gradient is different in the two geometries. When higher angles of attack were studied for the hemisphere-cylinder, a more complicated topological structure, not seen in the present study, was produced.

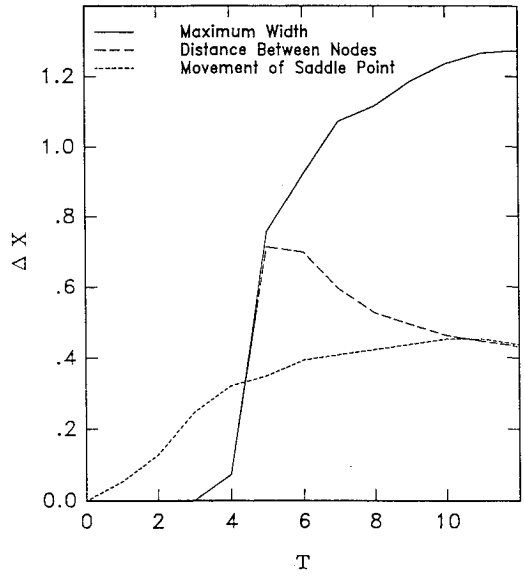

Fig. 6 Temporal growth of the owl-face separation.

Table 1 Topological development of the separation structure

T	T^*	Topology
0.0	0.0	Flow is fully attached with no singular points.
0.10	0.13	Onset of node and saddle along centerline.
0.50	0.64	Saddle of reattachment splits into two saddles and a node.
0.50–4.0	0.64–5.1	Saddles move spanwise away from the centerline.
4.0	5.1	Saddles reach sidewalls and each becomes two half-saddles. Node of separation splits into a saddle and two nodes.
4.0–5.0	5.1–6.4	Primary nodal points gradually develop to foci and move downstream and outward.
5.0	6.4	Spanwise vortex shedding begins near side walls.
5.0–6.0	6.4–7.6	Primary foci continue to move downstream but now move inward toward the centerline.
6.0	7.6	Vortex shedding occurs across the entire span.

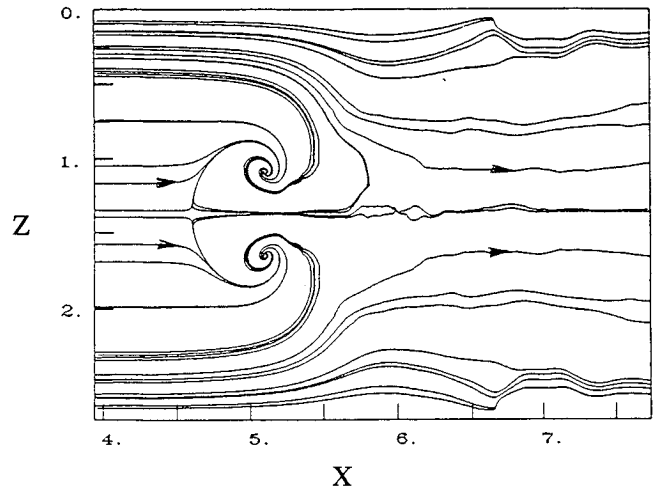

Fig. 7a Streamlines of the velocity projections in the X-Z plane at $Y = 0.02$ from the test wall; $T = 8.0$.

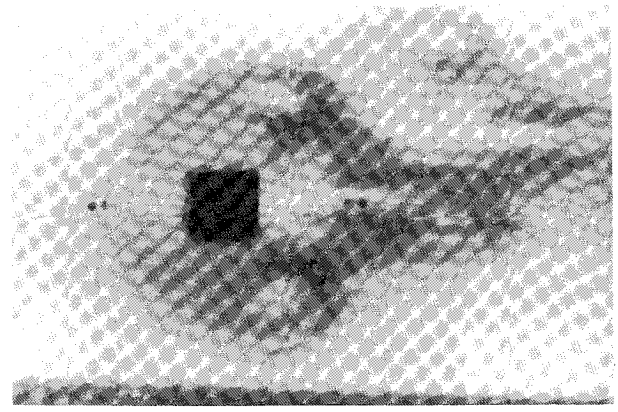

Fig. 7b Experimental dye visualization of developed separation (from HRR).

C. Three-Dimensional Flow Structure

Several different methods were used to study the structure of the three-dimensional separation. In this section, streamline projections of the velocity vector in a plane, three-dimensional streamlines, and vorticity lines produced from the computational results will be presented.

The separation structure obtained from the present computation was compared with the dye visualization from the ex-

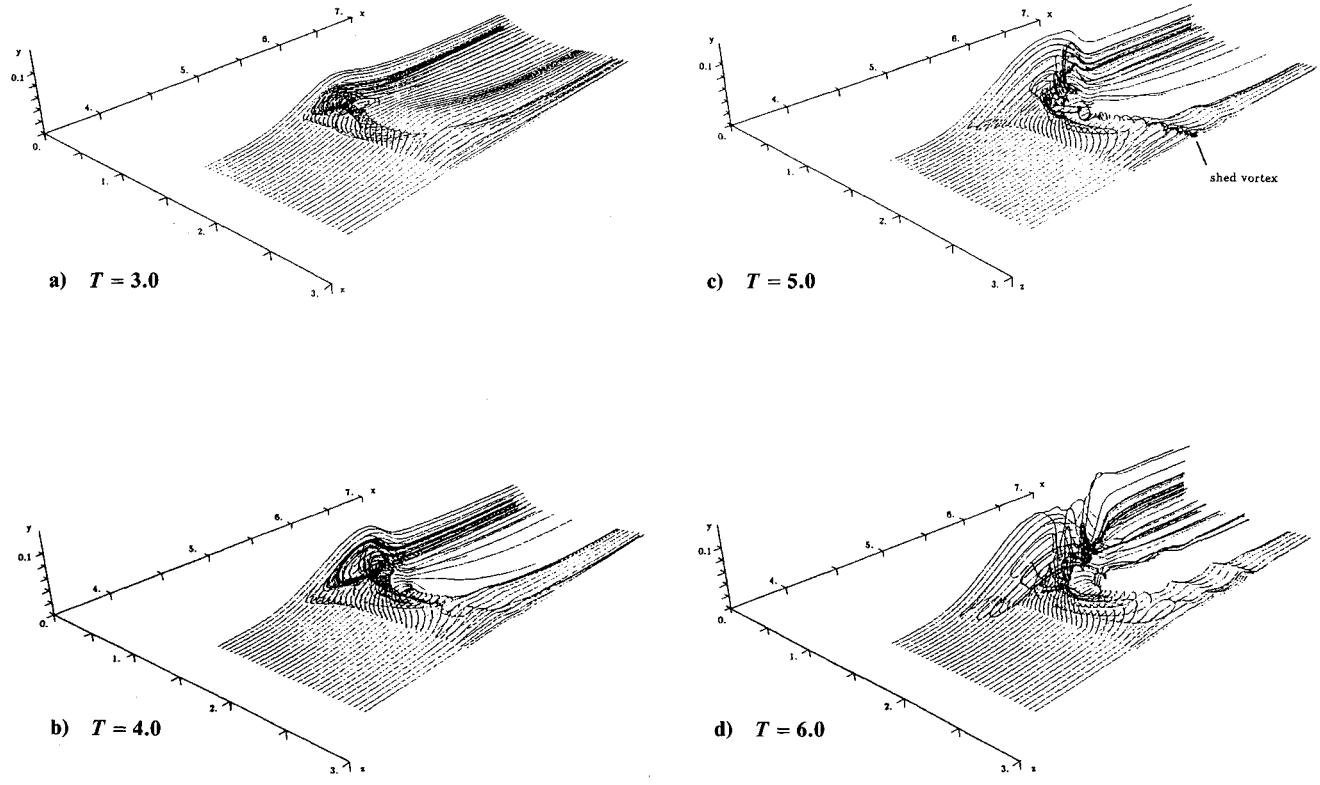

Fig. 8 Three-dimensional instantaneous streamlines.

periment of HRR. The separation structure of the numerical simulation was examined at $Y = 0.02$ for comparison since the flow structure marked by dye in the experiment was slightly above the wall. In this horizontal plane, the attached boundary-layer velocity is 10% of the freestream. Since the horizontal plane was close to the test wall, the normal velocity was much smaller than the streamwise and spanwise velocities. The streamlines produced by the velocity projection onto this plane were therefore equivalent to the actual streamlines. In Fig. 7a, the streamlines of the projected velocity vectors show that the flow does not reverse near the sidewalls in this plane. The spanwise separation, therefore, extends only a slight distance away from the wall. The dye visualization in HRR (Fig. 7b) found the steady-state separation to have a similar structure. The saddle point of separation and the primary nodes on either side of the centerline were observed in both the computational and experimental results. From the dye visualization photographs, a separation width of 3.5 ± 0.05 suction port widths was determined, which is in good agreement with 3.6 suction port widths found from the numerical study.

The velocity lines in Fig. 7 suggest the development of a separation that has been called an "owl-face of the first kind" by Perry and Chong.[12] The three-dimensional streamlines and the streamlines along the centerline also confirmed that the separation was an "owl-face of the first kind." The limiting streamlines (Fig. 5d), however, show a topological structure referred to as an "owl-face of the second kind" by Perry and Chong with saddle points at the channel sidewalls. The method of Perry and Chong is able to describe the global separation structure but not the near-wall structure. For this reason, it was found that the computational streamlines slightly away from the wall should be used to identify the three-dimensional flowfield structure as classified by Perry and Chong. Using the computational results at $T = 3.0$ and 4.0, the topology before the onset of vortex shedding was identified as a U separation.

The separation structure defined by the limiting streamlines can be seen by the development of the streamlines in three dimensions (Fig. 8). Streamlines are shown that originate at two different locations, upstream of the separation and in the vortex core that extends across the channel. For clarity, streamlines are shown for only half of the channel. The strong adverse pressure gradient at the center of the channel causes the separation to develop first at that location (Fig. 8a). The low momentum fluid near the wall reverses to create a vortex that rotates in a clockwise direction as shown. As the spanwise vortex becomes stronger (Fig. 8b), streamlines from upstream are entrained across most of the channel near the reattachment line. Fluid is drawn into the spanwise separation, moves toward the centerline due to the cross-stream pressure gradient, and is expelled near the centerline. As the separation grows (Fig. 8c), the vortex at the centerline moves downstream creating a bend that allows interaction of the vortex with itself. In addition, shedding is seen from the thin separation that extends across the span of the channel. Shedding is not observed from the free shear layer zone at the centerline, although velocity measurements indicate that the centerline flow contains periodic oscillations. When the vortex lifts from the wall (Fig. 8d), the free shear layer does not reattach but becomes unstable. Vortex shedding now occurs across the entire span. The full-field view provided by the streamlines confirms many observations from the two-dimensional visualizations described previously.

From the limiting streamlines (Fig. 5) the primary vortex was found to remain stationary. Only slight temporal fluctuations of the developed primary vortex were noted as each secondary vortex was shed from the entire primary vortex and propagated downstream. As seen in Fig. 8d, the secondary vortex began to shed first from the side walls.

As the head of the vortex moves downstream, the vortex legs are stretched and the free shear layer is lifted due to the upward flow between the vortex legs. This occurs for both the primary vortex and the vortex that is shed and propagates downstream. "Streamlines" that trace the projection of the velocity in a cross-stream plane are shown in Fig. 9 at $T = 6.0$. The length scale normal to the wall has been enlarged five times to highlight the near-wall structure. The streamlines show the cross section of one vortex that has shed from the primary separation. The vortex is cut four times by the cross-sectional plane. The streamlines near the centerline indicate a

strong interaction of the bent vortex with itself, which causes the vortex to lift away from the wall. The vortex halves move toward the centerline due to image vortices created by the wall. The clockwise-rotating vortex seen in cross section at $Z = 0.5$ is the vortex that shed from the spanwise separation.

The sketch in Fig. 10 gives an interpretation of the separation structure that is consistent with the characteristics revealed by the streamlines and vorticity lines (not shown) from the computation. Boundary-layer separation is present along the entire width of the channel, but near the sidewalls the separation remains very close to the test surface. The vortex bundle that comprises the primary vortex originates at the sidewalls and remains near the test wall until the foci are reached. At the foci of the primary separation, the vortex lifts and bends downstream. The vortex lines become tightly bound together as they lift from the wall, indicating a strengthening of the vorticity. Vortex shedding causes a vortex bundle to detach and travel downstream while retaining a shape similar to the primary vortex. The surface topology of the primary vortex remains nearly stationary during the shedding of the secondary vortex. One vortex line is anchored at each node and acts as the backbone of the separation. The lifted legs of the primary vortex and each shed vortex are wrapped around the anchored vortex line.

V. Separation Decay

The decay of the separation structure was studied upon impulsive removal of the adverse pressure gradient. The suction was removed at three different times in the separation development, and the decay of separation back to attached flow was studied. For the first case, suction is removed at $T = 1.68$ when the separation is in the early topological state of two nodes along the centerline. The second case examines the decay of the "owl-faced" separation found at $T = 5.04$. At this stage, vortex shedding has started along the thin spanwise separation across the entire channel, but no effect is yet

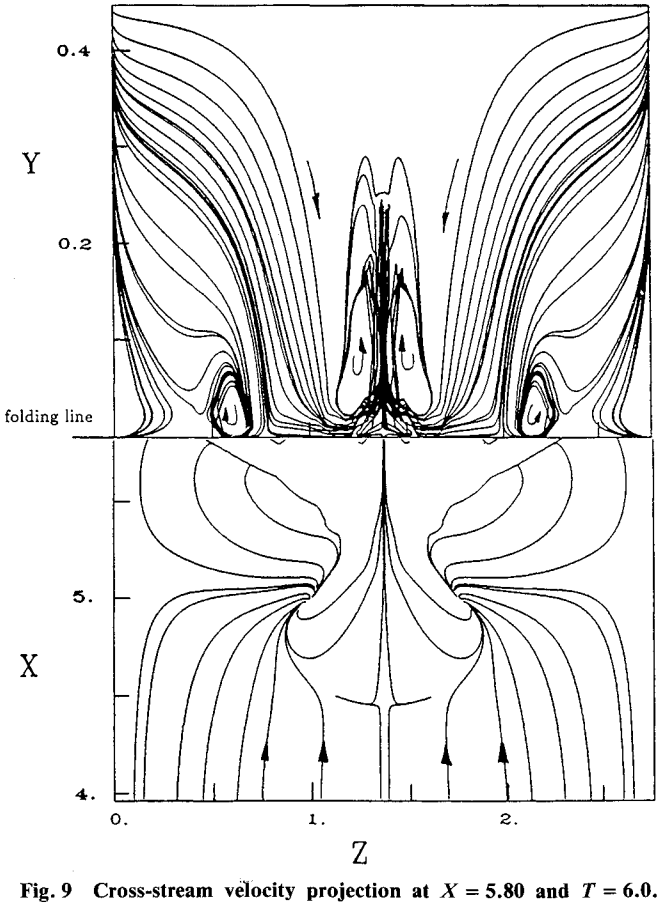

Fig. 9 Cross-stream velocity projection at $X = 5.80$ and $T = 6.0$. Limiting streamline results show the location of the X-Z plane.

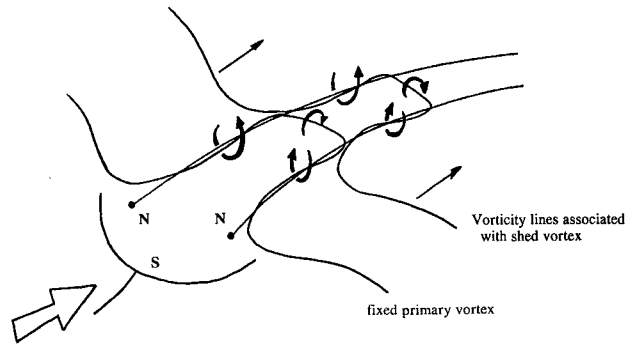

Fig. 10 Proposed schematic of the flow structure.

observed at the centerline. The third case considers the decay of the separation at $T = 8.40$ when vortex shedding takes place along the centerline. Refer to Table 1 for a summary of the topological development.

In case 1, the separated boundary layer rapidly returns to an attached, two-dimensional boundary layer when the adverse pressure gradient is removed. Retaining the adverse pressure gradient for a longer length of time in cases 2 and 3 creates a condition where the boundary layer does not quickly return to the previous Blasius conditions when the adverse pressure gradient is removed. The "owl-faced" separation quickly returned to an attached boundary layer, but a distinct three-dimensional boundary-layer flow persisted through the computations. For cases 2 and 3, the boundary-layer separation is catastrophic, and an attached boundary layer cannot be quickly recovered. These results give an indication of the time response required in any successful active boundary-layer control system. The active control must sense separation and correct the adverse pressure gradient so that the separation can be quickly removed.

Velocity histories along the centerline at two streamwise locations are shown in Fig. 3 for the decay of cases 2 and 3. The entire velocity history for the separation development is also shown. The sudden change in the velocity histories that occurs when the adverse pressure gradient is removed is due to the rapid response of the inviscid flow. For case 2, vortex shedding does not occur along the centerline before the adverse pressure gradient is removed. After the pressure gradient is removed, however, oscillations are present along the centerline at $X = 5.65$ (Fig. 3b). The frequency of oscillation is twice the shedding frequency found for the growth of the three-dimensional separation. In case 3, the pressure gradient is removed after shedding commences along the centerline. The frequency of oscillation for the separation decay was the same as for the separation growth. The shedding frequency of the free shear layer that remains after the "owl-faced" separation decays is therefore greatly affected by the stage of the developing separation when the pressure gradient is removed.

VI. Conclusions

The development and decay of a three-dimensional separation produced by an externally applied, three-dimensional, adverse pressure gradient was studied computationally. The flow conditions were the same as in the experiment of HRR. A well-defined three-dimensional pressure gradient was applied to an otherwise two-dimensional Blasius boundary layer. When the adverse pressure gradient was impulsively applied, the separation structure passed through several different topologies before reaching an "owl-face of the first kind" as described by Perry and Chong. Unlike an owl-faced structure created on a body at angle of attack, a thin separated region extended across the entire channel due to the effect of the adverse pressure gradient present across the entire span of the channel. As the separation developed, the free shear layer became unstable and periodic shedding occurred.

The Strouhal number for the shedding of vortices was determined from the computational velocity histories to be 0.0136. This compares well with the Strouhal number of 0.0134 found experimentally during the development of the separation. Although these two initial vortex shedding frequencies compare well with each other, the quasisteady-state shedding frequency determined from the experiment is lower than the initial shedding frequency. It is conjectured that the transition to turbulence of the free shear layer causes a decrease in the shedding frequency.

The adverse pressure gradient was removed, at three different times during the separation development. In all cases, the owl-faced separation was quickly reduced. When the pressure gradient was removed during the early separation growth, a Blasius boundary layer was soon restored. For cases where the pressure gradient was removed after the separation had further developed, the decay of the unsteadiness and three-dimensionality of the shear layer was much slower.

Acknowledgments

This research has been supported by the Office of Naval Research through Contracts N00014-84-K-0232 and N00014-90-J-1169. Computer facilities were provided by the Numerical Aerodynamic Simulation facility at NASA Ames Research Center. These contributions are gratefully acknowledged.

References

[1]Prandtl, L., "Uber Flüssigkeitsbewegung bei sehr kleiner Reibung," *Proceedings of the Third International Mathematics Congress,* Heidelberg, Germany, 1904, pp. 484–491. English Translation, NACA TM 452.

[2]Henk, R. W., Reynolds, W. C., and Reed, H. L., "An Experimental Investigation of the Fluid Mechanics of an Unsteady, Three-Dimensional Separation," Dept. of Mechanical Engineering, Stanford Univ., Rept. TF-49, Stanford, CA, Aug. 1990.

[3]Maskell, E. C., "Flow Separation in Three Dimensions," Royal Aircraft Establishment, Rept. Aero 2565, Nov. 1955.

[4]Oswatitsch, K., "Die Ablösungsbedingung von Grenzschichten," *Grenzschichtforschung,* edited by H. Goertler, Springer-Verlag, Berlin, Germany, 1958, pp. 357–367.

[5]Legendre, R., "Séparation de l'écoulement laminaire tridimensionnel," *La Recherche Aéronautique,* Vol. 54, Nov.–Dec. 1956, pp. 3–8.

[6]Davey, A., "Boundary-Layer Flow at a Saddle Point of Attachment," *Journal of Fluid Mechanics,* Vol. 10, Pt. 4, June 1961, pp. 593–610.

[7]Lighthill, M. J., "Introduction. Boundary Layer Theory," *Laminar Boundary Layers,* edited by L. Rosenhead, Vol. II, Oxford Univ. Press, Oxford, England, UK, 1963, pp. 72–82.

[8]Wang, K. C., "On the Disputes About Open Separation," AIAA Paper 83-0296, Jan. 1983.

[9]Tobak, M., and Peake, D. J., "Topology of Three-Dimensional Separated Flows," *Annual Review of Fluid Mechanics,* Vol. 14, 1982, pp. 61–85.

[10]Perry, A. E., and Fairlie, B. D., "Critical Points in Flow Patterns," *Advanced Geophysics,* Vol. 18B, 1974, pp. 299–315.

[11]Hunt, J. C. R., Abell, C. J., Peterka, J. A., and Woo, H., "Kinematical Studies of the Flow Around Free or Surface-Mounted Obstacles: Applying Topology to Flow Visualization," *Journal of Fluid Mechanics,* Vol. 86, Pt. 1, May 1978, pp. 179–200.

[12]Perry, A. E., and Chong, M. S., "A Series-Expansion Study of the Navier-Stokes Equations with Application to Three-Dimensional Separation Patterns," *Journal of Fluid Mechanics,* Vol. 173, Dec. 1986, pp. 207–223.

[13]Peake, D. J., and Tobak, M., "Three-Dimensional Interactions and Vortical Flows with Emphasis on High Speeds," AGARDograph 252, July 1980.

[14]Bippes, H., "Experimental Investigation of Topological Structures in 3-Dimensional Separated Flow," *Boundary-Layer Separation, Proceedings of the IUTAM Symposium* (London, Aug. 26–28, 1986), edited by F. T. Smith and S. N. Brown, Springer-Verlag, Berlin, Germany, 1987, pp. 379–381.

[15]Werlé, H., "Separation on Axisymmetrical Bodies at Low Speed," *La Recherche Aéronautique,* Vol. 90, Sept.–Oct. 1962, pp. 3–14.

[16]Peake, D. J., and Tobak, M., "Three-Dimensional Flows about Simple Components at Angle of Attack," NASA TM 84226, March 1982.

[17]Perry, A. E., and Chong, M. S., "A Description of Eddying Motions and Flow Patterns Using Critical-Point Concepts," *Annual Review of Fluid Mechanics,* Vol. 19, 1987, pp. 125–155.

[18]Ying, S. X., Schiff, L. B., and Steger, J. L., "A Numerical Study of Three-Dimensional Separated Flow Past a Hemisphere Cylinder," AIAA Paper 87-1207, June 1987.

[19]Wang, K. C., and Hsieh, T., "Separation Patterns and Flow Structures About a Hemisphere-Cylinder at High Incidences," AIAA Paper 92-2712, June 1992.

[20]McCroskey, W. J., "Some Current Research in Unsteady Fluid Dynamics," *Journal of Fluids Engineering,* Vol. 99, No. 1, 1977, pp. 8–38.

[21]Telionis, D. P., "Review—Unsteady Boundary Layers, Separated and Attached," *Journal of Fluids Engineering,* Vol. 101, No. 1, 1979, pp. 29–43.

[22]Reynolds, W. C., and Carr, L. W., "Review of Unsteady, Driven, Separated Flows," AIAA Paper 85-0527, March 1985.

[23]Moffatt, H. K., and Tsinober, A. (eds.), "Topological Fluid Mechanics," *Proceedings of the IUTAM Symposium* (Cambridge, England, UK, 1989). Cambridge Univ. Press, Cambridge, England, UK, 1990.

[24]Dallmann, U., "Analysis of Simulations of Topologically Changing Three-Dimensional Separated Flows," *Separated Flows and Jets, Proceedings of the IUTAM Symposium* (Novosibirsk, USSR, July 1990), edited by V. V. Kozlov and A. V. Dovgal, Springer-Verlag, New York, 1991, pp. 167–171.

[25]Dallmann, U., "Three-Dimensional Vortex Structures and Vorticity Topology," *Fluid Dynamics Research,* Vol. 3, March 1988, pp. 183–189.

[26]Pauley, L. L., Moin, P., and Reynolds, W. C., "The Structure of Two-Dimensional Separation," *Journal of Fluid Mechanics,* Vol. 220, Nov. 1990, pp. 397–411.

[27]Kim, J., and Moin, P., "Application of a Fractional-Step Method to Incompressible Navier-Stokes Equations," *Journal of Computational Physics,* Vol. 59, No. 2, 1985, pp. 308–323.

[28]Yates, L. A., and Chapman, G. T., "Streamlines, Vorticity Lines, and Vortices Around Three-Dimensional Bodies," *AIAA Journal,* Vol. 30, No. 7, 1992, pp. 1819–1826.

[29]Mack, L. M., "Transition Prediction and Linear Stability Theory," AGARD CP-224, Oct. 1977.

[30]Narasimha, R., "The Laminar-Turbulent Transition Zone in the Boundary Layer," *Progress in Aerospace Sciences,* Vol. 22, 1985, pp. 29–80.

[31]Hui, W. H., and Tobak, M., "Topology of Steady and Unsteady Incompressible Three-Dimensional Separated Flows," *Continuum Mechanics and Its Applications,* edited by G. A. Graham and S. K. Malik, Hemisphere, New York, 1989, pp. 519–541.